

SAIR: Cost-Efficient Multi-Stage ML Pipeline Autoscaling via In-Context Reinforcement Learning

Jianchang Su¹, Yifan Zhang¹, Shengkai Lin², Shizhen Zhao², Yusheng Zheng³, Yiwei Yang³, Wei Zhang^{1,*}

¹University of Connecticut

²Shanghai Jiao Tong University

³University of California, Santa Cruz

Abstract

Multi-stage ML inference pipelines are difficult to autoscale due to heterogeneous resources, cross-stage coupling, and dynamic bottleneck migration. We present SAIR, an autoscaling framework that uses an LLM as an in-context reinforcement learning controller, improving its policy online from reward-labeled interaction histories without gradient updates. SAIR combines Pareto-dominance reward shaping with a provable separation margin, surprisal-guided experience retrieval for context efficiency, and fine-grained GPU rate control via user-space CUDA interception. We provide regret analysis decomposing error into retrieval coverage and LLM selection components. On four ML serving pipelines under three workload patterns, SAIR achieves the best or tied-best P99 latency and effective resource cost among deployed baselines, improving P99 by up to 50% and reducing effective cost by up to 97% (under GPU rate-control assumptions), with 86% bottleneck detection accuracy and no offline training.

1 Introduction

Modern machine learning serving systems increasingly decompose monolithic inference into multi-stage pipelines to optimize resource utilization across heterogeneous hardware [Crankshaw et al. \[2017, 2020\]](#), [Gunnasekaran et al. \[2022\]](#). A typical pipeline consists of CPU/memory-bound preprocessing (data transformation), GPU-accelerated inference (neural network execution), and CPU/memory-bound postprocessing (result aggregation), connected through message queues. While this architecture improves efficiency and modularity, it creates

complex autoscaling challenges that existing approaches cannot adequately address.

The fundamental difficulty stems from three interconnected phenomena. First, *dynamic bottleneck migration* causes the performance-limiting stage to shift based on workload intensity, resource allocation, and model characteristics. A preprocessing bottleneck at low load may migrate to inference at high load, then to postprocessing as inference scales. Second, *cross-stage coupling* means that scaling decisions propagate through the pipeline with variable delays, creating feedback loops that destabilize reactive controllers. Third, *temporal causality obscures root causes*: high GPU utilization might indicate GPU shortage or downstream congestion, and distinguishing symptoms from causes requires causal reasoning across time.

Current autoscaling approaches fall into three categories, each inadequate for multi-stage pipelines. *Rule-based* autoscalers like Kubernetes HPA [The Kubernetes Authors \[2026\]](#) and VPA operate on single-stage metrics with threshold-based policies, lacking cross-stage reasoning. When GPU utilization exceeds 80%, HPA adds replicas even if the root cause is downstream congestion. *Learning-based* autoscalers [Rzadca et al. \[2020\]](#), [Qiu et al. \[2020, 2023\]](#) use deep RL from historical data but require thousands of offline training episodes, environment instrumentation, and per-application reward engineering, and fail to generalize under distribution shift. *Heuristic-based* approaches combine rules with domain knowledge but require extensive manual tuning and encode workload assumptions that break when patterns change.

We propose SAIR, a fundamentally different approach: using Large Language Models as *in-context reinforcement learning* (ICRL) agents that learn scaling policies through experience accumulation without

*Corresponding author: wei.13.zhang@uconn.edu

parameter updates. Unlike traditional RL, ICRL stores knowledge in the LLM’s context window rather than in neural network weights, requiring no gradient computation. This enables: (1) zero-shot deployment without offline training; (2) compositional generalization over novel context-action combinations; and (3) continuous improvement through experience accumulation while remaining fully interpretable. Our contributions:

- We formulate multi-stage pipeline autoscaling as a contextual bandit with an evolving Pareto frontier in context, and introduce SAIR, which uses LLMs as in-context RL agents with Pareto-based reward shaping that balances latency and cost without manual threshold tuning.
- We provide regret bounds via a decomposition into retrieval coverage error and LLM selection error, prove Pareto reward frontier separation, and establish sample complexity bounds for bottleneck identification.
- We design continuous GPU rate control via user-space `LD_PRELOAD` interception of CUDA calls, enabling fine-grained resource actuation with sub-second response time.
- We validate SAIR on four ML serving pipelines. SAIR achieves the best or tied-best effective cost and P99 latency among all deployed baselines in every setting, with 86% bottleneck detection accuracy.

2 Related Works

Autoscaling for Cloud Systems. Autopilot [Rzadca et al. \[2020\]](#) pioneered ML-based vertical scaling at Google but requires extensive training data. FIRM [Qiu et al. \[2020\]](#) and AWARE [Qiu et al. \[2023\]](#) apply deep RL to autoscaling with safety constraints but need thousands of offline training episodes. Sinan [Zhang et al. \[2021\]](#) uses ML models for QoS-aware microservice management but requires offline profiling and per-application model training. HPA [The Kubernetes Authors \[2026\]](#) remains the industry standard but lacks cross-stage reasoning. SAIR requires no offline training and handles multi-stage coordination natively.

ML Inference Serving and LLM Scheduling. Clipper [Crankshaw et al. \[2017\]](#) introduced adaptive batching, InferLine [Crankshaw et al. \[2020\]](#) uses queuing-theoretic models, and Cocktail [Gunasekaran et al. \[2022\]](#) addresses multi-dimensional optimization. For LLM serving, Orca [Yu et al. \[2022\]](#) introduced iteration-level scheduling for transformer-based generation, vLLM [Kwon et al. \[2023\]](#) proposed PagedAttention for efficient KV-cache memory management, Lluminx [Sun et al. \[2024\]](#) enables dynamic scheduling via live migration, QLM [Patke et al. \[2024\]](#) introduces queue-level SLO management, and Chiron [Patke et al. \[2025\]](#) proposes hierarchical autoscaling. These systems focus on scheduling within serving clusters; SAIR addresses multi-stage *pipeline* autoscaling across heterogeneous stages and uses an LLM as the control policy rather than as the workload.

In-Context Learning, RL, and Example Selection. LLMs can learn from few-shot examples without parameter updates [Brown et al. \[2020\]](#), [Garg et al. \[2022\]](#), [Xie et al. \[2021\]](#). For RL, Algorithm Distillation [Laskin et al. \[2022\]](#) and supervised pretraining [Lee et al. \[2023\]](#) enable in-context RL. Krishnamurthy et al. [Krishnamurthy et al. \[2024\]](#) showed LLMs do not robustly explore in-context without interventions; Song et al. [Song et al. \[2025\]](#) demonstrated that reward feedback alone can drive ICRL. SAIR addresses known failure modes through forced probes, positive-only memory, and Pareto reward margin (0.2 separation). For example selection, KATE [Liu et al. \[2022\]](#) showed kNN-based retrieval improves ICL, and IDEAL [Zhang et al. \[2025\]](#) introduced influence-driven selective annotations. Our approach differs by selecting from a growing *experience buffer* and combining similarity with a surprisal term that captures information gain (Appendix B).

Multi-Objective Optimization and GPU Sharing. Multi-objective optimization has a rich history, with NSGA-II [Deb et al. \[2002\]](#) introducing fast non-dominated sorting and crowding distance for Pareto front approximation. Our Pareto-based reward uses hypervolume contribution [Zitzler and Thiele \[1998\]](#) to balance latency and cost without manual weight tuning; see Hayes et al. [Hayes et al. \[2021\]](#) for a survey of multi-objective RL. Unlike methods that learn a full Pareto policy, our LLM selects actions conditioned on a shaped scalar reward with provable frontier separation (Proposition 5.2). The surprisal score relates to Bayesian surprise [Itti and Baldi \[2005\]](#), formalized in Appendix B. For GPU sharing, Gandiva [Xiao et al. \[2018\]](#) introduced introspective scheduling with GPU time-slicing, AntMan [Xiao et al. \[2020\]](#) enables dynamic GPU co-location through fine-grained memory and computation management, Salus [Yu and Chowdhury \[2020\]](#) provides GPU sharing primitives for deep learning, and Dilu [Lv et al. \[2025\]](#) achieves

GPU resourcing-on-demand for serverless DL serving through introspective elasticity with two-dimensional co-scaling. Our approach is lighter-weight: a user-space CUDA interception library that throttles kernel launches via token-bucket rate limiting, requiring no kernel modifications or driver changes.

3 Problem Formulation

Consider an ML inference pipeline $\mathcal{S} = \{s_1, s_2, \dots, s_N\}$ with N stages connected through message queues. Each stage s_i processes requests with rate μ_i and maintains input queue Q_i . The end-to-end latency decomposes as $L_{e2e} = \sum_{i=1}^N (L_i^{proc} + L_i^{queue})$ where L_i^{proc} is processing latency and L_i^{queue} is queueing delay at stage i . Each stage has resource configuration $\mathbf{r}_i = (n_i, c_i, m_i, \rho_i)$ where $n_i \in \mathbb{Z}^+$ is replica count, c_i, m_i are CPU/memory allocations, and $\rho_i \in [0, 1]$ is GPU rate ratio.

We formalize multi-stage autoscaling as a *contextual bandit* problem, where each decision interval (default: 30 seconds) constitutes one round. We adopt a contextual bandit abstraction because the system reaches a quasi-steady-state within each interval: after a settling window, the reward $r_t = R(x_t, a_t)$ depends on the current context and action, not on the full trajectory history. The context $x_t \in \mathcal{X}$ captures pipeline metrics and the current Pareto frontier: $x_t = (\{\mathbf{r}_i, q_i, u_i^{cpu}, u_i^{gpu}, L_{p99}\}_{i=1}^N, \mathcal{P}_t)$ where \mathcal{P}_t is the Pareto frontier maintained at round t . Including \mathcal{P}_t in the context ensures $r_t = R(x_t, a_t)$ depends only on the round- t context and action, preserving the bandit structure. Actions are *discretized* scaling decisions: $\mathcal{A} = \prod_i \mathcal{A}_i$ with stage-specific action sets: for CPU stages, $\mathcal{A}_i^{cpu} = \{\Delta n_i, \Delta c_i, \Delta m_i\}$ with $\Delta n_i \in \{-1, 0, +1, +2\}$, $\Delta c_i \in \{-\gamma_c, 0, +\gamma_c\}$, $\Delta m_i \in \{-\gamma_m, 0, +\gamma_m\}$; for GPU stages, $\mathcal{A}_i^{gpu} = \{\Delta n_i, \Delta \rho_i\}$ with $\Delta \rho_i \in \{-0.1, 0, +0.1, +0.2\}$. After action a_t and a settling window, we observe reward r_t . We seek a policy $\pi : \mathcal{X} \rightarrow \mathcal{A}$ minimizing cumulative regret relative to the optimal context-dependent policy.

We make four assumptions that characterize the problem structure:

Assumption 3.1 (Bounded Reward Range). The shaped reward satisfies $|R_t| \leq R_{max}$ for all rounds. This holds because each reward component is normalized and clipped to a fixed range (see Algorithm 2 in Appendix E).

Assumption 3.2 (Bottleneck Identifiability). There exists a mapping $\phi : \mathcal{X} \rightarrow \{1, \dots, N\}$ identifying the

bottleneck stage such that scaling stage $\phi(x)$ yields expected reward improvement at least $\Delta > 0$, while scaling other stages yields improvement at most $\Delta/2$. This reflects queueing dynamics: in a tandem queue, the stage with highest utilization limits throughput, and scaling it yields the largest marginal gain.

Assumption 3.3 (Retrieval Coverage Error). Given context x_t , the experience selection returns a set \mathcal{E}_t that induces a candidate action set $\mathcal{A}(\mathcal{E}_t) \subseteq \mathcal{A}$. The *coverage gap* is

$$\xi_t = \max \left(0, \mathbb{E}[R(x_t, a_t^*)] - \max_{a \in \mathcal{A}(\mathcal{E}_t)} \mathbb{E}[R(x_t, a)] \right), \quad (1)$$

measuring how much optimality is lost because the retrieved context does not contain relevant action patterns.

Assumption 3.4 (LLM Selection Error on Retrieved Set). Conditioned on retrieved experiences \mathcal{E}_t , the LLM outputs $a_t \in \mathcal{A}(\mathcal{E}_t)$ such that

$$\max_{a \in \mathcal{A}(\mathcal{E}_t)} \mathbb{E}[R(x_t, a)] - \mathbb{E}[R(x_t, a_t)] \leq \eta_t \quad (2)$$

with probability at least $1 - \delta_{LLM}$. This captures the LLM’s bounded suboptimality *within* the actions suggested by retrieved experiences. The constraint $a_t \in \mathcal{A}(\mathcal{E}_t) \subseteq \mathcal{A}$ is enforced by design: SAIR presents a discrete action schema via structured JSON output and applies an action validator (Appendix D) that clamps any out-of-range proposal to the nearest feasible action in \mathcal{A} .

4 SAIR: In-Context RL for Autoscaling

In this section, we present SAIR, a scalable autoscaling approach for multi-stage pipelines based on in-context reinforcement learning (ICRL). We define ICRL as a learning paradigm where an LLM improves its policy by conditioning on accumulated experience tuples (x, a, r) from *online* system interactions, without any gradient-based parameter updates. SAIR is not offline trajectory distillation: it collects reward-labeled tuples from live deployment, and the reward signal directly drives future action selection through retrieval. Traditional RL stores learned knowledge in neural network parameters updated through gradient descent, requiring thousands of training episodes and suffering from catastrophic forgetting when distributions shift. ICRL instead stores knowledge as experience tuples in the LLM’s context window, enabling zero-shot deployment and continuous adaptation.

In-Context Reinforcement Learning. The core insight is that LLMs can learn effective policies from reward feedback provided entirely in-context, without parameter updates. Rather than learning a parametric policy $\pi_\theta(a|x)$ through gradient descent, we define the policy implicitly through the LLM’s conditional distribution:

$$\pi_{SAIR}(a|x) = P_{LLM}(a|x, \mathcal{E}_{1:M}) \quad (3)$$

where $\mathcal{E}_{1:M} = \{(x_i, a_i, r_i)\}_{i=1}^M$ are past episodes provided as in-context examples. The LLM conditions on these examples to identify patterns between pipeline contexts and effective scaling actions, improving action selection as more relevant experiences accumulate.

SAIR satisfies the ICRL definition because: (i) the agent accumulates (x, a, r) tuples from real system interactions, not from a fixed dataset; (ii) the policy π_{SAIR} improves as more relevant experiences are retrieved, as measured by decreasing coverage gap ξ_t (Theorem 5.1); and (iii) the reward signal drives action selection, not just the context. Recent work Krishnamurthy et al. [2024] shows that naive ICRL can fail at exploration; SAIR addresses this through forced probes (ϵ_t -greedy), positive-only memory (filtering noisy negative feedback), and Pareto reward margin (0.2 separation for action discrimination).

The LLM estimates expected reward through pattern matching and compositional reasoning. Given context x and candidate action a , the LLM: (1) identifies experiences with similar context features (latency profile, utilization pattern, queue depths); (2) examines the actions taken and resulting rewards in similar situations; (3) combines patterns through compositional reasoning to predict expected reward; and (4) expresses confidence based on similarity of retrieved experiences.

Pareto-Based Reward Shaping. Standard threshold-based rewards often lead to reactive policies that scale only after SLA violations occur, creating oscillations between under- and over-provisioning. We design a multi-objective reward function that encourages proactive scaling while balancing latency and cost. The total reward decomposes as:

$$R(x, a) = R_{latency} + R_{cost} + R_{SLA} + R_{proactive} + R_{pareto} \quad (4)$$

The latency component rewards improvement: $R_{latency} = w_L \cdot (L_{before} - L_{after})/L_{baseline}$. The cost component penalizes resource increase: $R_{cost} = -w_C \cdot (C_{after} - C_{before})/C_{budget}$. For SLA violations,

penalty grows quadratically to create urgency:

$$R_{SLA} = \begin{cases} -\left(\frac{L_{after}}{T_{SLA}}\right)^2 + 1 & \text{if } L_{after} > T_{SLA} \\ 0 & \text{otherwise} \end{cases} \quad (5)$$

For balancing the fundamental latency-cost tradeoff, we use Pareto-dominance-based reward shaping:

$$R_{pareto}(a) = \begin{cases} 1 + H(a) & \text{if } a \in \mathcal{P} \text{ (non-dominated)} \\ \frac{0.8}{1+d(a, \mathcal{P})} & \text{otherwise} \end{cases} \quad (6)$$

where \mathcal{P} is the current Pareto frontier maintained across all experiences, $H(a)$ is the hypervolume contribution of action a (measuring improvement to the frontier), and $d(a, \mathcal{P})$ is the Euclidean distance to the frontier in normalized objective space. Non-dominated solutions receive bonus reward proportional to their hypervolume contribution, encouraging exploration of the Pareto frontier. Dominated solutions receive reward inversely proportional to their distance from the frontier, providing gradient toward improvement.

The proactive scaling bonus encourages multi-stage coordinated scaling during violations:

$$R_{proactive} = \sigma(x) \cdot \mu(a) \cdot w_{proactive} \quad (7)$$

where $\sigma(x) = \max(0, L_{p99}/T_{SLA} - 1)$ is violation severity and $\mu(a) = \sum_i |\Delta n_i| + \alpha \sum_i (|\Delta c_i|/\gamma_c + |\Delta m_i|/\gamma_m + |\Delta \rho_i|) + \frac{1}{2}|\text{stages_scaled}|$ aggregates all action dimensions with $\alpha = 0.5$.

Surprisal-Based Experience Selection. Context window limitations (typically 8K–32K tokens) restrict the number of experiences that can be provided to the LLM. With potentially thousands of accumulated experiences, selecting the most informative subset is critical. We select M experiences from buffer \mathcal{D} maximizing information gain:

$$\mathcal{E}^* = \arg \max_{\mathcal{E} \subset \mathcal{D}, |\mathcal{E}|=M} I(\mathcal{E}; \pi^* | x_{curr}) \quad (8)$$

We approximate this using a leave-one-out surprisal score:

$$\text{score}(e) = \text{sim}(x_e, x_{curr}) \cdot \underbrace{[r_e - \mathbb{E}[r | \mathcal{D}_{-e}]]}_{\text{surprise}} \quad (9)$$

where $\text{sim}(x_e, x_{curr}) = \exp(-\|x_e - x_{curr}\|^2/2\sigma^2)$ ensures relevance and the surprise term identifies experiences with unexpected outcomes. With diversity regularization:

$$\mathcal{E}^* = \arg \max_{\mathcal{E}} \left[\sum_{e \in \mathcal{E}} \text{score}(e) - \lambda_{div} \sum_{e_i, e_j \in \mathcal{E}} \text{sim}(e_i, e_j) \right] \quad (10)$$

The first term is modular and the pairwise penalty is supermodular, making the combined objective submodular but *not* monotone (the diversity penalty can decrease marginal gain). The classic $(1 - 1/e)$ guarantee of Nemhauser et al. Nemhauser et al. [1978] requires monotonicity and thus does not directly apply. We use greedy selection as a practical heuristic; non-monotone submodular maximization under cardinality constraints admits a randomized $(1/e)$ -approximation, but we find that deterministic greedy selection with $\lambda_{div} = 0.1$ produces diverse, high-quality experience sets that empirically outperform both random selection and pure similarity-based retrieval (Table 1).

Continuous GPU Control via CUDA Interception. Traditional GPU scaling is discrete (add/remove replicas) with 30–60s startup latency. We enable continuous GPU control through user-space CUDA interception. Our approach intercepts CUDA kernel launches via `LD_PRELOAD`, implementing token-bucket throttling with rate ratio $\rho \in [0, 1]$:

$$\text{tokens}_\tau = T_{max} \cdot \rho \quad (11)$$

where each window τ (10ms) grants tokens proportional to ρ . Kernel launches consume tokens proportional to their parallelism (grid blocks); when exhausted, launches block until refill. This achieves three properties critical for effective RL: (1) *Fine-grained action space*: The mechanism supports continuous ρ , but SAIR uses bounded discrete increments $\Delta\rho_i \in \{-0.1, 0, +0.1, +0.2\}$ as a safety layer; (2) *Immediate effect*: Rate changes via Unix socket take effect within milliseconds (measured overhead <2ms); (3) *Instant reversibility*: Can increase or decrease ρ instantly, unlike replica scaling with asymmetric scale-up/down times.

GPU utilization is normalized to quota: $u_{quota} = \min(1, u_{actual}/\rho)$, ensuring Assumption 3.2 holds regardless of rate limit.

Positive-Only Episode Filtering. We store only episodes with positive reward ($r > r_{min}$) to bias the context toward successful scaling decisions. This serves two purposes: it prevents the agent from learning bad patterns from failed attempts (whose complex causes are difficult to generalize from), and it improves the signal-to-noise ratio, ensuring limited context budget is spent on informative successes. Approximately 30% of decisions yield negative reward and are filtered out.

SAIR Algorithm. Algorithm 1 presents the complete decision loop integrating all components. Each iteration: (1) collects current context from metrics; (2) selects experiences via surprisal-based selection; (3) with probability

Algorithm 1 SAIR Agent Decision Loop

```

1: Input: LLM  $\mathcal{L}$ , context size  $M$ , reward threshold
    $r_{min}$ , initial exploration  $\epsilon_0$ 
2: Initialize: Episode buffer  $\mathcal{D} \leftarrow \emptyset$ , Pareto frontier
    $\mathcal{P} \leftarrow \emptyset$ ,  $\epsilon_t \leftarrow \epsilon_0$ 
3: for each decision step  $t = 1, 2, \dots$  do
4:   Observe current context  $x_t$  from metrics collector
5:    $\mathcal{E}_t \leftarrow \text{SelectExperiences}(\mathcal{D}, x_t, M)$  {Eq. 8}
6:   With prob.  $\epsilon_t$ :  $a_t \leftarrow \text{RandomProbe}()$  {Forced
   exploration}
7:   Otherwise:  $a_t \leftarrow \mathcal{L}(\mathcal{E}_t, x_t, \text{constraints})$ 
8:   Execute action  $a_t$ ; wait settling window; observe
   reward  $r_t$ 
9:    $r_t \leftarrow \text{ParetoReward}(x_t, a_t, \mathcal{P})$  {Eq. 5}
10:  if  $r_t > r_{min}$  then
11:     $\mathcal{D} \leftarrow \mathcal{D} \cup \{(x_t, a_t, r_t)\}$  {Positive-only}
12:  end if
13:  Update Pareto frontier:  $\mathcal{P} \leftarrow \text{UpdateFrontier}(\mathcal{P}, L_t, C_t)$ 
14:   $\epsilon_t \leftarrow \max(\epsilon_{min}, \epsilon_t \cdot \lambda)$  {Decay exploration}
15: end for

```

ϵ_t , takes a forced exploration probe, otherwise queries the LLM; (4) executes the action via Kubernetes API (CPU stages) or direct socket (GPU rate); (5) computes Pareto-based reward; and (6) stores positive episodes.

5 Theoretical Analysis

We provide theoretical guarantees for SAIR’s in-context RL loop. Since the pipeline reaches a quasi-steady-state within each decision interval, we analyze using a contextual bandit abstraction. The regret definition applies round-wise regardless of whether contexts are stochastic, adversarial, or history-dependent: at each round t , we compare $\pi(x_t)$ to $a_t^* = \arg \max_a R(x_t, a)$ for that specific context x_t . Full proofs are in Appendix A.

Theorem 5.1 (SAIR Regret Bound). *Under Assumptions 3.1–3.4, let ϵ_t be the exploration probability at round t . SAIR achieves:*

$$\text{Regret}(T) \leq \sum_{t=1}^T (1 - \epsilon_t)(\xi_t + \eta_t) + \left(\sum_{t=1}^T \epsilon_t + \delta_{LLM} T \right) R_{max} \quad (12)$$

where ξ_t is retrieval coverage gap, η_t is LLM selection error, and $\sum_t \epsilon_t$ accounts for exploration rounds.

Proof sketch. With probability ϵ_t the agent explores (at most R_{max} regret); otherwise the LLM policy incurs

coverage gap ξ_t plus selection error η_t (with δ_{LLM} failure probability). Summing over T rounds yields the bound. Full proof in Appendix A.

Proposition 5.2 (Pareto Reward: Frontier Separation). *Under Eq. 6 with normalized objectives $\tilde{L}, \tilde{C} \in [0, 1]$ and hypervolume computed with respect to the reference point $(1, 1)$, any non-dominated action receives reward at least 1, and any dominated action receives reward at most 0.8. Therefore,*

$$a \in \mathcal{P}, b \notin \mathcal{P} \Rightarrow R_{\text{pareto}}(a) - R_{\text{pareto}}(b) \geq 0.2. \quad (13)$$

Furthermore, with normalized objectives, $H(a) \in [0, 1]$, so $R_{\text{pareto}}(a) \in [0, 2]$, satisfying Assumption 3.1.

Proof. Non-dominated actions receive $R_{\text{pareto}}(a) = 1 + H(a) \geq 1$. Dominated actions have $d(b, \mathcal{P}) > 0$, so $R_{\text{pareto}}(b) = 0.8/(1 + d(b, \mathcal{P})) < 0.8$. The margin of at least 0.2 ensures the LLM can reliably separate non-dominated from dominated actions given sufficient context. Boundedness follows from objective normalization: $\tilde{L} = L/L_{\max}, \tilde{C} = C/C_{\max}$, yielding $H(a) \in [0, 1]$.

Theorem 5.3 (Bottleneck Detection Sample Complexity). *Under Assumption 3.2, suppose the forced exploration probes in Algorithm 1 generate m scaling experiments per stage under stationary reward distributions. Then SAIR correctly identifies the bottleneck stage with probability at least $1 - \delta$ using $m = O(R_{\max}^2 N^2 / \Delta^2 \cdot \log(N/\delta))$ probes.*

Proof sketch. By Hoeffding’s inequality with gap Δ and union bound over $O(N^2)$ stage pairs. Our empirical 86% accuracy is consistent with this bound for $N = 4$. Full proof in Appendix A.

Lemma 5.4 (Bottleneck Marginal Gain). *In a tandem queueing system with stages having utilizations u_1, \dots, u_N , the stage $i^* = \arg \max_i u_i$ with highest utilization yields the largest marginal latency reduction when scaled.*

This queueing-theoretic result justifies Assumption 3.2: pipeline bottlenecks create observable symptoms (high utilization, queue buildup) that distinguish them from non-bottleneck stages.

Lemma 5.5 (Retrieval Coverage Under Smoothness). *Suppose $\mathbb{E}[R(x, a)]$ is L -Lipschitz in x for each fixed a . If \mathcal{E}_t contains an experience (x_e, a_e, r_e) with $\|x_e - x_t\| \leq d_t$ and $a_e \in \arg \max_a \mathbb{E}[R(x_e, a)]$, then $\xi_t \leq 2L \cdot d_t$.*

Proof. Let $a_t^* \in \arg \max_a \mathbb{E}[R(x_t, a)]$. Then $\mathbb{E}[R(x_t, a_t^*)] \leq \mathbb{E}[R(x_e, a_t^*)] + Ld_t \leq \mathbb{E}[R(x_e, a_e)] + Ld_t \leq \mathbb{E}[R(x_t, a_e)] + 2Ld_t$, where the first and third steps use Lipschitz continuity and the second uses optimality of a_e at x_e . Since $a_e \in \mathcal{A}(\mathcal{E}_t)$, we have $\max_{a \in \mathcal{A}(\mathcal{E}_t)} \mathbb{E}[R(x_t, a)] \geq \mathbb{E}[R(x_t, a_e)]$, so $\xi_t \leq 2Ld_t$.

Corollary 5.6 (Sublinear Cumulative Coverage Regret). *Suppose contexts x_t lie in a bounded d -dimensional subspace of \mathcal{X} and the experience buffer \mathcal{D} grows by at least one entry per round. Under the conditions of Lemma 5.5, the nearest-neighbor distance satisfies $d_t = O(|\mathcal{D}_t|^{-1/d})$ by standard covering-number arguments, so $\sum_{t=1}^T \xi_t = O(L \cdot T^{1-1/d})$, which is sublinear in T for any finite d .*

This connects surprisal-based selection to coverage quality: the diversity term (Eq. 8) reduces expected retrieval distance d_t by ensuring spatial coverage, while the similarity term ensures retrieved experiences are close to x_t . Corollary 5.6 guarantees that SAIR’s policy improves over time as the buffer grows.

Discussion. Theorem 5.1 provides a system-aligned performance accounting: each term maps to a SAIR component, yielding actionable design knobs:

- **Coverage gap** ξ_t : Reduced by surprisal-based selection (Eq. 8) with diversity regularization. As the buffer grows, ξ_t decreases (Corollary 5.6).
- **LLM selection error** η_t : Reduced by constrained JSON output, action validator (Table 2), and Pareto reward margin (Proposition 5.2, 0.2 separation).
- **Exploration penalty** $\sum_t \epsilon_t$: Controlled by decaying ϵ_t ($\lambda = 0.95, \epsilon_{\min} = 0.05$).

The ablation study confirms asymmetric Pareto weighting is critical: equal weights cause -3.9% throughput, cost-focused weights cause $+27\%$ latency (Table 1).

6 Experiments

We assess SAIR against widely deployed auto-scalers. Our experiments span four ML serving pipelines with diverse latency profiles from 60ms to 18 seconds, evaluating on three workload patterns. Each experiment processes $\sim 1M$ requests with 3 random seeds; we report mean values.

6.1 Experimental Setup

Hardware. Kubernetes cluster with $2 \times$ NVIDIA RTX A6000 GPUs (49GB each), 64 CPU cores, 256GB memory.

Applications. We evaluate four ML serving pipelines spanning diverse computational profiles:

- **Image Classification:** MobileNetV2 with CPU-heavy preprocessing (image decoding, resizing, normalization), GPU inference, and lightweight post-processing.
- **NLP Analysis:** BERT-based text analysis with balanced CPU/GPU workload and dynamic bottleneck migration.
- **Text Generation:** Transformer decoder with GPU-intensive autoregressive generation creating variable latency.
- **Video Analysis:** Multi-frame processing with high memory requirements and 10–20s latency profile.

Workload Patterns. Three patterns stress different autoscaling capabilities: *Poisson* (steady-state with random arrivals), *Ramp* (gradually increasing load), and *Burst* (periodic traffic spikes).

Baselines. We compare against four production autoscalers:

- **Static:** Fixed allocation (1 replica per stage).
- **HPA-CPU:** Kubernetes HPA with 70% CPU utilization target, 60s stabilization window.
- **VPA:** Vertical Pod Autoscaler for resource sizing, update mode `Auto`.
- **Threshold:** Rule-based P99 latency thresholds at 100ms (CPU) / 200ms (GPU), 60s cooldown.

All baselines use per-application tuned parameters; HPA and Threshold targets were swept over $\{50, 60, 70, 80\}\%$ and $\{50, 100, 200, 500\}\text{ms}$ respectively, selecting best-performing values. Learning-based controllers (FIRM [Qiu et al. \[2020\]](#), AWARE [Qiu et al. \[2023\]](#)) require offline pretraining, making them impractical for zero-shot evaluation.

Metrics. (1) P99 end-to-end latency; (2) effective resource cost per 1M requests. We distinguish two cost models. *Billable cost* reflects whole-GPU pricing: $C_{bill} = \sum_{i \in \text{CPU}} n_i c_i p_{cpu} + \sum_{i \in \text{GPU}} n_i p_{gpu}$, where

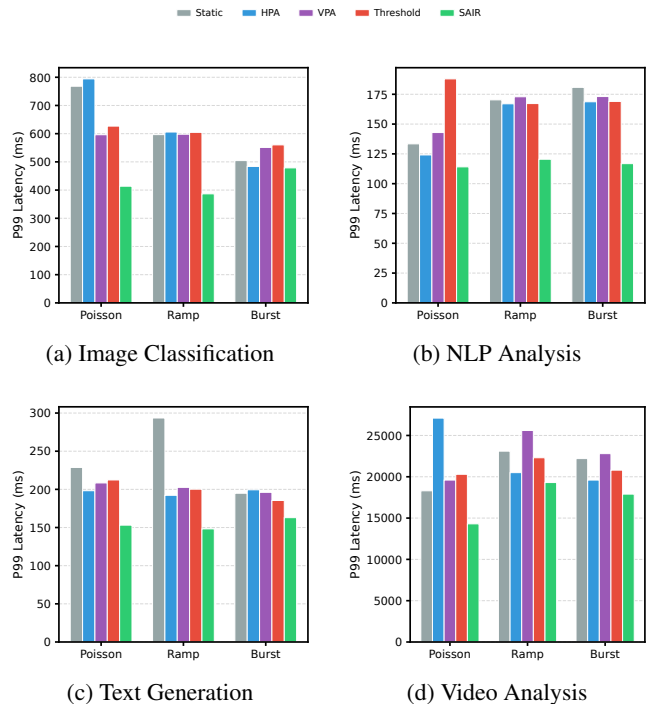


Figure 1: P99 latency comparison across applications and patterns.

each GPU incurs full cost regardless of utilization. *Effective cost* accounts for GPU rate control: $C_{eff} = \sum_{i \in \text{CPU}} n_i c_i p_{cpu} + \sum_{i \in \text{GPU}} n_i \rho_i p_{gpu}$, where throttling to $\rho_i < 1$ frees capacity for co-located workloads. We report C_{eff} using AWS on-demand pricing (p3.2xlarge GPU, m5.xlarge CPU); this metric is appropriate when GPUs are shared via time-slicing or MIG. In single-tenant deployments where GPU sharing is unavailable, the cost reduction from rate control is limited to enabling fewer replicas through better utilization.

6.2 Main Results

Figure 1 and Figure 2 present P99 latency and normalized cost across all configurations (4 applications \times 3 workload patterns). Raw cost data is provided in Appendix G.

SAIR achieves the lowest P99 latency in every configuration (Figure 1): Image Classification 35–46% (proactive CPU scaling at preprocessing bottleneck), NLP Analysis 8–31% (handling dynamic bottleneck migration), Text Generation 12–50% (GPU rate limiting for variable generation latency), and Video Analysis 6–47% (the only method successfully processing this high-latency pipeline).

SAIR also achieves the best effective cost (Figure 2), with 30–60% effective cost reduction relative to the next-

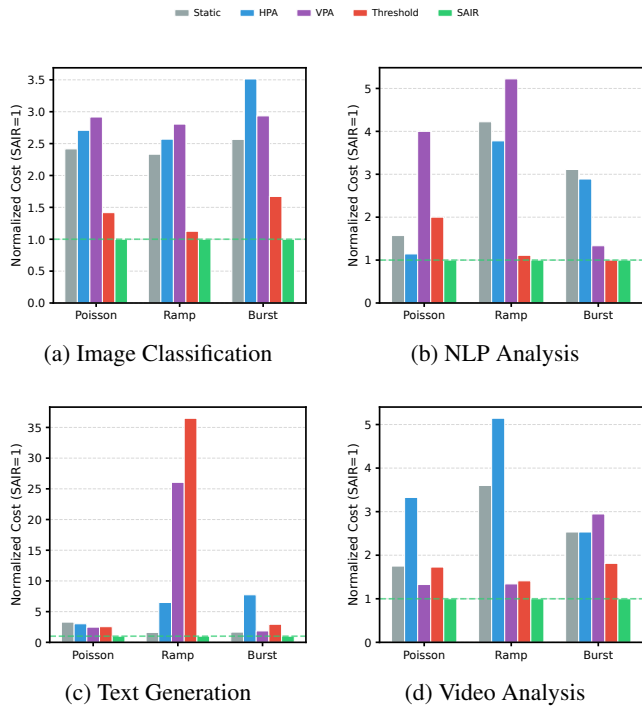


Figure 2: Normalized cost comparison (SAIR=1). Values >1 indicate higher cost.

best baseline and up to 81% relative to HPA on Video Analysis.

6.3 Bottleneck Detection

We evaluate bottleneck detection on 200 test scenarios with known ground-truth bottlenecks (Figure 3). SAIR achieves **86% overall accuracy** (172/200 correct), with 89–92% on single-stage bottlenecks and 71% on multi-stage bottlenecks ($2.8 \times$ random baseline of 25%). The high single-stage accuracy enables targeted scaling, avoiding wasteful scaling of non-bottleneck stages.

6.4 Ablation Study

We conduct a systematic ablation study on the Image Classification pipeline, disabling or modifying key components of SAIR. We organize 8 configurations across three categories: in-context learning (ICL), reward shaping, and architecture. Each configuration is run with 3 seeds and results are averaged. Table 1 summarizes results; Figure 4 visualizes throughput and P99 latency.

In-Context Learning. Removing in-context experiences entirely (No ICL) causes -1.7% throughput and $+17\%$ P99 latency (1054 ms vs. 902 ms), validating that experience accumulation benefits decision quality. Figure 5 shows that Full SAIR maintains stability while No ICL

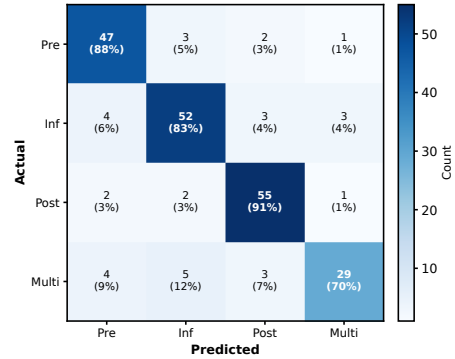


Figure 3: Bottleneck detection confusion matrix (200 test cases). Overall accuracy: 86%. Per-class metrics in Appendix H.

Table 1: Ablation study (3 seeds). $\Delta\%$ vs Full SAIR.

Config	Tput	P99	ΔT	ΔL
Full SAIR	84.0	902	–	–
No ICL	82.6	1054	-1.7	$+16.8$
Store All	83.0	1012	-1.2	$+12.1$
Linear Pen.	80.6	962	-4.1	$+6.6$
No Bonus	81.7	1006	-2.7	$+11.4$
Equal Wt.	80.7	936	-3.9	$+3.7$
Cost Focus	81.4	1149	-3.1	$+27.4$
Pre Only	81.9	1054	-2.5	$+16.8$

shows more erratic behavior. Storing all episodes rather than positive-only filtering degrades by $-1.2\% / +12\%$, confirming that negative examples introduce noise.

Reward Shaping. Linear SLA penalty causes the largest degradation (-4.1%), demonstrating that the quadratic penalty (Eq. 4) creates essential urgency during SLA violations. Cost-focused weights (-3.1%) cause the worst P99 latency (1149 ms, $+27\%$), as the agent over-optimizes for cost. Equal weights (-3.9%) and no scaling bonus (-2.7% , $+11\%$ latency) confirm asymmetric Pareto weighting is critical.

Architecture. Single-stage scaling (Pre Only) causes -2.5% throughput and $+17\%$ latency, confirming that multi-stage coordination is essential. The single-stage variant cannot identify cross-stage bottlenecks.

Key Findings. All 7 ablations degrade from Full SAIR, validating each component’s contribution. Reward shaping shows the largest impact (-2.7% to -4.1% throughput), confirming the Pareto-based reward structure is the most critical component. Multi-stage coordination is essential (-2.5%), and in-context learning provides consistent benefits (-1.7%).

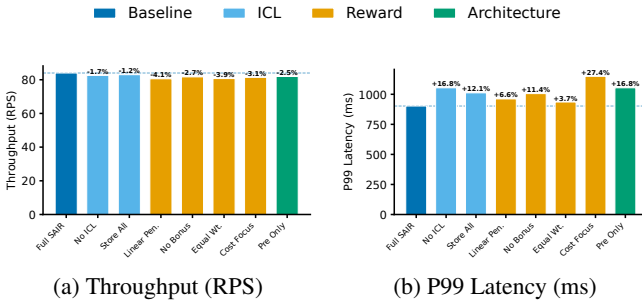


Figure 4: Ablation study: all ablations degrade from Full SAIR baseline (dashed line).

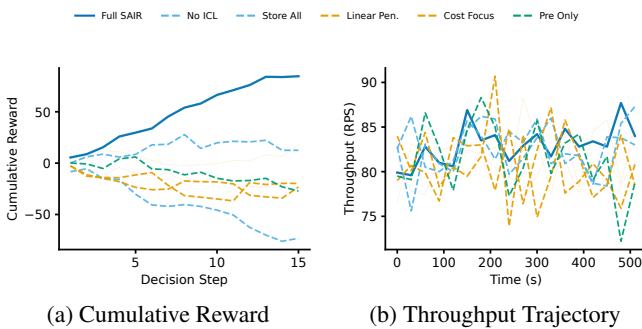


Figure 5: Learning dynamics. Full SAIR (solid) accumulates higher reward and achieves more stable throughput than ablated variants (dashed).

7 Discussion

When Does SAIR Excel? SAIR provides largest benefits when: (1) workloads have complex cross-stage dependencies that rule-based autoscalers cannot reason about; (2) bottlenecks migrate dynamically; (3) no training data is available for learning-based approaches. For simple, stable workloads, traditional approaches may suffice.

Limitations and Threats to Validity. *LLM latency:* Decision time of 1–2s limits sub-second control loops; SAIR targets minute-scale autoscaling. *Context window:* Limited to 15–20 experiences, addressed through surprisal-based selection. *Cost model:* Effective cost assumes GPU sharing; in single-tenant mode, cost savings are smaller. *Cluster scale:* Our 2-GPU cluster validates the approach but does not test large-scale scheduling effects.

Reproducibility. SAIR is model-agnostic in interface: the JSON action schema, action validator, experience retrieval, and reward computation are independent of the LLM backend. The LLM affects only η_t in Theorem 5.1; the retrieval coverage ξ_t depends solely on the buffer and selection algorithm. We provide complete prompt

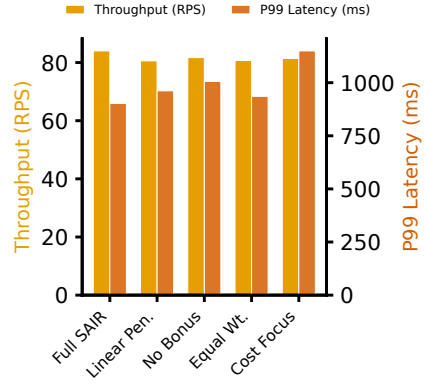


Figure 6: Reward component sensitivity. All ablations degrade from baseline.

templates (Appendix I), validator constraints (Table 2), reward pseudocode (Algorithm 2), and hyperparameters (Appendix F). LLM outputs are validated and clamped before execution.

Future Directions. *Hierarchical control:* Combine fast local controllers (HPA) with strategic LLM decisions (SAIR). *Predictive scaling:* Use LLMs to forecast workload patterns. *Multi-cluster:* Extend to geo-distributed deployments.

8 Conclusion

We presented SAIR, demonstrating that LLMs can perform effective in-context reinforcement learning for multi-stage ML pipeline autoscaling without offline training or parameter updates. SAIR achieves the best or tied-best effective cost and P99 latency in every setting (up to 50% P99 improvement, 97% effective cost reduction relative to Threshold) through four contributions: in-context RL with regret bounds decomposing retrieval coverage and LLM selection error, Pareto-based reward shaping with provable frontier separation, surprisal-based experience selection with sublinear coverage regret, and continuous GPU control via CUDA interception. An ablation study (8 configurations, 3 seeds) confirms reward shaping is most critical (−4.1%), followed by multi-stage coordination (−2.5%) and in-context learning (−1.7%).

References

Tom Brown, Benjamin Mann, Nick Ryder, Melanie Subbiah, Jared D Kaplan, Prafulla Dhariwal, Arvind Neelakantan, Pranav Shyam, Girish Sastry, Amanda Askell, et al. Language models are few-shot learners.

Advances in neural information processing systems, 33:1877–1901, 2020.

Daniel Crankshaw, Xin Wang, Giulio Zhou, Michael J Franklin, Joseph E Gonzalez, and Ion Stoica. Clipper: A {Low-Latency} online prediction serving system. In *14th USENIX Symposium on Networked Systems Design and Implementation (NSDI 17)*, pages 613–627, 2017.

Daniel Crankshaw, Gur-Eyal Sela, Xiangxi Mo, Corey Zumar, Ion Stoica, Joseph Gonzalez, and Alexey Tumanov. Inferline: latency-aware provisioning and scaling for prediction serving pipelines. In *Proceedings of the 11th ACM Symposium on Cloud Computing*, pages 477–491, 2020.

Kalyanmoy Deb, Amrit Pratap, Sameer Agarwal, and TAMT Meyarivan. A fast and elitist multiobjective genetic algorithm: Nsga-ii. *IEEE transactions on evolutionary computation*, 6(2):182–197, 2002.

Shivam Garg, Dimitris Tsipras, Percy S Liang, and Gregory Valiant. What can transformers learn in-context? a case study of simple function classes. volume 35, pages 30583–30598, 2022.

Jashwant Raj Gunasekaran, Cyan Subhra Mishra, Prashanth Thinakaran, Bikash Sharma, Mahmut Taylan Kandemir, and Chita R Das. Cocktail: A multidimensional optimization for model serving in cloud. In *19th USENIX Symposium on Networked Systems Design and Implementation (NSDI 22)*, pages 1041–1057, 2022.

Conor F Hayes, Roxana Rădulescu, Eugenio Bargiacchi, Johan Källström, Matthew Macfarlane, Mathieu Reymond, Timothy Verstraeten, Luisa M Zintgraf, Richard Dazeley, Fredrik Heintz, et al. A practical guide to multi-objective reinforcement learning and planning. *arXiv preprint arXiv:2103.09568*, 2021.

Laurent Itti and Pierre Baldi. Bayesian surprise attracts human attention. *Advances in neural information processing systems*, 18, 2005.

Omar Khattab, Arnav Singhvi, Paridhi Maheshwari, Zhiyuan Zhang, Keshav Santhanam, Sri Vardhamanan, Saiful Haq, Ashutosh Sharma, Thomas T Joshi, Hanna Moazam, et al. Dspy: Compiling declarative language model calls into self-improving pipelines. *arXiv preprint arXiv:2310.03714*, 2023.

Akshay Krishnamurthy, Keegan Harris, Dylan J Foster, Cyril Zhang, and Aleksandrs Slivkins. Can large language models explore in-context? *Advances in Neural Information Processing Systems*, 37:120124–120158, 2024.

Woosuk Kwon, Zhuohan Li, Siyuan Zhuang, Ying Sheng, Lianmin Zheng, Cody Hao Yu, Joseph Gonzalez, Hao Zhang, and Ion Stoica. Efficient memory management for large language model serving with pagedattention. In *Proceedings of the 29th symposium on operating systems principles*, pages 611–626, 2023.

Michael Laskin, Luyu Wang, Junhyuk Oh, Emilio Parisotto, Stephen Spencer, Richie Steigerwald, DJ Strouse, Steven Hansen, Angelos Filos, Ethan Brooks, et al. In-context reinforcement learning with algorithm distillation. *arXiv preprint arXiv:2210.14215*, 2022.

Jonathan Lee, Annie Xie, Aldo Pacchiano, Yash Chandak, Chelsea Finn, Ofir Nachum, and Emma Brunskill. Supervised pretraining can learn in-context reinforcement learning. *Advances in Neural Information Processing Systems*, 36:43057–43083, 2023.

Jiachang Liu, Dinghan Shen, Yizhe Zhang, William B Dolan, Lawrence Carin, and Weizhu Chen. What makes good in-context examples for gpt-3? In *Proceedings of Deep Learning Inside Out (DeeLIO 2022): The 3rd workshop on knowledge extraction and integration for deep learning architectures*, pages 100–114, 2022.

Cunchi Lv, Xiao Shi, Zhengyu Lei, Jinyue Huang, Wenting Tan, Xiaohui Zheng, and Xiaofang Zhao. Dilu: Enabling gpu resourcing-on-demand for serverless dl serving via introspective elasticity. In *Proceedings of the 30th ACM International Conference on Architectural Support for Programming Languages and Operating Systems, Volume 1*, pages 311–325, 2025.

George L Nemhauser, Laurence A Wolsey, and Marshall L Fisher. An analysis of approximations for maximizing submodular set functions—i. *Mathematical programming*, 14(1):265–294, 1978.

Archit Patke, Dhemath Reddy, Saurabh Jha, Haoran Qiu, Christian Pinto, Chandra Narayanaswami, Zbigniew Kalbarczyk, and Ravishankar Iyer. Queue management for slo-oriented large language model serving. In *Proceedings of the 2024 ACM Symposium on Cloud Computing*, pages 18–35, 2024.

Archit Patke, Dhemath Reddy, Saurabh Jha, Chandra Narayanaswami, Zbigniew Kalbarczyk, and Ravishankar Iyer. Hierarchical autoscaling for large language model serving with chiron. *arXiv preprint arXiv:2501.08090*, 2025.

Haoran Qiu, Subho S Banerjee, Saurabh Jha, Zbigniew T Kalbarczyk, and Ravishankar K Iyer. {FIRM}: An intelligent fine-grained resource management framework for {SLO-Oriented} microservices. In *14th USENIX symposium on operating systems design and implementation (OSDI 20)*, pages 805–825, 2020.

Haoran Qiu, Weichao Mao, Chen Wang, Hubertus Franke, Alaa Youssef, Zbigniew T Kalbarczyk, Tamer Başar, and Ravishankar K Iyer. {AWARE}: Automate workload autoscaling with reinforcement learning in production cloud systems. In *2023 USENIX Annual Technical Conference (USENIX ATC 23)*, pages 387–402, 2023.

Krzysztof Rzadca, Paweł Findeisen, Jacek Swiderski, Przemysław Zych, Przemysław Broniek, Jarek Kusmirek, Paweł Nowak, Beata Strack, Piotr Witkowski, Steven Hand, et al. Autopilot: workload autoscaling at google. In *Proceedings of the Fifteenth European Conference on Computer Systems*, pages 1–16, 2020.

Kefan Song, Amir Moeini, Peng Wang, Lei Gong, Rohan Chandra, Shangtong Zhang, and Yanjun Qi. Reward is enough: Llms are in-context reinforcement learners. *arXiv preprint arXiv:2506.06303*, 2025.

Biao Sun, Ziming Huang, Hanyu Zhao, Wencong Xiao, Xinyi Zhang, Yong Li, and Wei Lin. Llumnix: Dynamic scheduling for large language model serving. In *18th USENIX symposium on operating systems design and implementation (OSDI 24)*, pages 173–191, 2024.

The Kubernetes Authors. Kubernetes, 2026. URL <https://kubernetes.io/>. Homepage: “Production-Grade Container Orchestration”.

Wencong Xiao, Romil Bhardwaj, Ramachandran Ramjee, Muthian Sivathanu, Nipun Kwatra, Zhenhua Han, Pratyush Patel, Xuan Peng, Hanyu Zhao, Quanlu Zhang, et al. Gandiva: Introspective cluster scheduling for deep learning. In *13th USENIX Symposium on Operating Systems Design and Implementation (OSDI 18)*, pages 595–610, 2018.

Wencong Xiao, Shiru Ren, Yong Li, Yang Zhang, Pengyang Hou, Zhi Li, Yihui Feng, Wei Lin, and Yangqing Jia. {AntMan}: Dynamic scaling on {GPU} clusters for deep learning. In *14th USENIX Symposium on Operating Systems Design and Implementation (OSDI 20)*, pages 533–548, 2020.

Sang Michael Xie, Aditi Raghunathan, Percy Liang, and Tengyu Ma. An explanation of in-context learning as implicit bayesian inference. 2021.

Gyeong-In Yu, Joo Seong Jeong, Geon-Woo Kim, Soo-jeong Kim, and Byung-Gon Chun. Orca: A distributed serving system for {Transformer-Based} generative models. In *16th USENIX Symposium on Operating Systems Design and Implementation (OSDI 22)*, pages 521–538, 2022.

Peifeng Yu and Mosharaf Chowdhury. Fine-grained gpu sharing primitives for deep learning applications. *Proceedings of Machine Learning and Systems*, 2:98–111, 2020.

Shaokun Zhang, Xiaobo Xia, Zhaoqing Wang, Ling-Hao Chen, Jiale Liu, Qingyun Wu, and Tongliang Liu. Ideal: Influence-driven selective annotations empower in-context learners in large language models, 2025. URL <https://arxiv.org/abs/2310.10873>.

Yanqi Zhang, Weizhe Hua, Zhuangzhuang Zhou, G Edward Suh, and Christina Delimitrou. Sinan: Ml-based and qos-aware resource management for cloud microservices. In *Proceedings of the 26th ACM international conference on architectural support for programming languages and operating systems*, pages 167–181, 2021.

Eckart Zitzler and Lothar Thiele. Multiobjective optimization using evolutionary algorithms—a comparative case study. In *International conference on parallel problem solving from nature*, pages 292–301. Springer, 1998.

A Proof Details

A.1 Proof of Theorem 5.1 (SAIR Regret Bound)

Proof. Let $E_t \in \{0, 1\}$ indicate whether round t is a forced exploration round (probability ϵ_t). When $E_t = 1$, the agent takes a random probe and incurs at most R_{max} regret (Assumption 3.1).

When $E_t = 0$ (LLM policy), the per-round regret decomposes as:

$$\mathbb{E}[R(x_t, a_t^*)] - \mathbb{E}[R(x_t, a_t)] \quad (14)$$

$$= \underbrace{\mathbb{E}[R(x_t, a_t^*)] - \max_{a \in \mathcal{A}(\mathcal{E}_t)} \mathbb{E}[R(x_t, a)]}_{\xi_t \text{ (coverage gap, Assumption 3.3)}} \quad (15)$$

$$+ \underbrace{\max_{a \in \mathcal{A}(\mathcal{E}_t)} \mathbb{E}[R(x_t, a)] - \mathbb{E}[R(x_t, a_t)]}_{\leq \eta_t \text{ w.p. } 1 - \delta_{LLM} \text{ (Assumption 3.4)}} \quad (16)$$

With probability $1 - \delta_{LLM}$, the LLM-policy regret is at most $\xi_t + \eta_t$. With probability δ_{LLM} , the regret is bounded by R_{max} .

Combining exploration and exploitation rounds over T rounds:

$$\begin{aligned} \text{Regret}(T) &\leq \sum_t [\epsilon_t R_{max} + (1 - \epsilon_t)((\xi_t + \eta_t) + \delta_{LLM} R_{max})] \\ &\leq \sum_t (1 - \epsilon_t)(\xi_t + \eta_t) + (\sum_t \epsilon_t + \delta_{LLM} T) R_{max} \end{aligned} \quad (17)$$

The decomposition shows that SAIR's regret depends on three terms: (i) retrieval coverage quality ξ_t , reducible through surprisal-based selection; (ii) LLM selection quality η_t , reducible through prompt constraints and action validation; and (iii) exploration cost $\sum_t \epsilon_t \cdot R_{max}$, controlled by decaying ϵ_t . \square

A.2 Proof of Proposition 5.2 (Frontier Separation)

Proof. We normalize objectives to $\tilde{L} = L/L_{max} \in [0, 1]$ and $\tilde{C} = C/C_{max} \in [0, 1]$, and compute hypervolume with respect to the reference point $(1, 1)$.

Non-dominated actions ($a \in \mathcal{P}$): $R_{pareto}(a) = 1 + H(a)$. Since $H(a) \geq 0$ for any point on the frontier, $R_{pareto}(a) \geq 1$. With normalized objectives and reference point $(1, 1)$, $H(a) \leq 1$, so $R_{pareto}(a) \leq 2$.

Dominated actions ($b \notin \mathcal{P}$): $R_{pareto}(b) = 0.8/(1 + d(b, \mathcal{P}))$. Since $d(b, \mathcal{P}) > 0$ for any dominated action, $R_{pareto}(b) < 0.8$.

Separation margin: For any $a \in \mathcal{P}$ and $b \notin \mathcal{P}$:

$$R_{pareto}(a) - R_{pareto}(b) \geq 1 - 0.8 = 0.2 \quad (18)$$

Boundedness: $R_{pareto} \in [0, 2]$, so $R_{max} = 2$ in the total reward, satisfying Assumption 3.1. \square

A.3 Proof of Theorem 5.3 (Sample Complexity)

Proof. The proof applies to the *forced exploration subsequence* of Algorithm 1, where the agent takes random probing actions with probability ϵ_t .

Step 1: Signal from probes. Under Assumption 3.2, probing the true bottleneck $\phi(x)$ yields reward improvement at least Δ , while probing non-bottleneck stage $j \neq \phi(x)$ yields improvement at most $\Delta/2$. We assume reward distributions are stationary during the probing period.

Step 2: Concentration for stage identification. After m probes scaling stage i , let \hat{r}_i be the empirical mean reward improvement. By Hoeffding's inequality for bounded rewards (Assumption 3.1):

$$\mathbb{P} \left[|\hat{r}_i - \mathbb{E}[r_i]| > \frac{\Delta}{4} \right] \leq 2 \exp \left(-\frac{m\Delta^2}{8R_{max}^2} \right) \quad (19)$$

Step 3: Union bound over stage pairs. To correctly identify the bottleneck, we need $\hat{r}_{\phi(x)} > \hat{r}_j + \Delta/2$ for all $j \neq \phi(x)$. With concentration $\Delta/4$ for each stage, this holds when true gaps are at least $\Delta/2$.

Union bound over all $\binom{N}{2} \leq N^2/2$ pairs gives failure probability:

$$\mathbb{P}[\text{error}] \leq N^2 \cdot \exp\left(-\frac{m\Delta^2}{8R_{\max}^2}\right) \quad (20)$$

Setting this to target failure probability δ and solving for m :

$$m = O\left(\frac{R_{\max}^2 N^2}{\Delta^2} \log \frac{N}{\delta}\right) \quad (21)$$

The total number of decision steps needed is $T_{\text{explore}} = m \cdot N/\bar{\epsilon}$ where $\bar{\epsilon}$ is the average exploration rate, since each probe is assigned to a stage uniformly. \square

B Surprisal Score as Information Gain Proxy

We justify the leave-one-out surprisal score (Eq. 7) as a proxy for information gain under a simple Gaussian model.

Lemma B.1 (Surprisal-Information Gain Connection). *Suppose rewards in a local neighborhood of context space follow $r \sim \mathcal{N}(\mu, \sigma^2)$ with conjugate prior $\mu \sim \mathcal{N}(\mu_0, \tau^2)$. Let \mathcal{D}_{-e} denote the buffer excluding experience e , and let μ_{-e} be the posterior mean given \mathcal{D}_{-e} . Then the KL divergence between posteriors (a standard measure of Bayesian surprise) satisfies:*

$$D_{KL}(p(\mu | \mathcal{D}) \| p(\mu | \mathcal{D}_{-e})) \propto (r_e - \mu_{-e})^2. \quad (22)$$

Therefore, the leave-one-out residual $|r_e - \mathbb{E}[r | \mathcal{D}_{-e}]|$ is monotone in information gain under this model.

Proof. Under the conjugate Gaussian model, the posterior given n observations is $\mathcal{N}(\mu_n, \sigma_n^2)$ where $\mu_n = (\tau^{-2}\mu_0 + \sigma^{-2} \sum r_i)/(\tau^{-2} + n\sigma^{-2})$. The KL divergence between two Gaussians is $D_{KL} = \frac{1}{2}[(\mu_n - \mu_{n-1})^2/\sigma_n^2 + \sigma_{n-1}^2/\sigma_n^2 - 1 + \log(\sigma_n^2/\sigma_{n-1}^2)]$. Since σ_n^2 and σ_{n-1}^2 depend only on n (not on observations), the only observation-dependent term is $(\mu_n - \mu_{n-1})^2 \propto (r_e - \mu_{-e})^2$. \square

This provides theoretical grounding for the heuristic: experiences with large leave-one-out residuals correspond to high information gain about the local reward structure, making them most useful for in-context RL.

C System Implementation Details

Kubernetes Operator. SAIR is implemented as a Kubernetes operator using the Kopf framework. The operator watches PipelineAutoscaler custom resources and manages the SAIR agent lifecycle. The agent runs as a sidecar container alongside the pipeline stages.

Metrics Collection. Context observation uses three sources: (1) GPU metrics via `LD_PRELOAD` library that intercepts CUDA calls and reports active/idle time to a Unix socket; (2) CPU metrics via cgroup accounting from Kubernetes metrics API; (3) Queue depth via monitor endpoint.

Action Execution. CPU stage scaling uses Kubernetes Deployment API with rolling updates. GPU rate control uses direct Unix socket communication with the rate-limiting library, bypassing Kubernetes for millisecond response time.

LLM Integration. SAIR can use any model like GPT5.1-mini/Claude Haiku/Local Qwen 32B with temperature 1.0 (required for reasoning models) and structured output via DSPy. The prompt includes: current context (metrics), selected experiences (5–15 episodes), and constraints (resource limits, cost budget). The LLM returns a structured JSON action that is parsed and validated before execution.

Table 2: Action validation constraints applied to every LLM decision.

Constraint	Value
Max replica change $ \Delta n_i $ per step (all)	≤ 2
Max CPU change $ \Delta c_i $ per step, γ_c (CPU)	500 m
Max memory change $ \Delta m_i $ per step, γ_m (CPU)	256 MB
Max GPU rate change $ \Delta \rho_i $ per step (GPU)	≤ 0.2
Min GPU rate ratio ρ_{min} (GPU)	0.1
Max replicas per stage n_{max}	8
Cooldown between scale-ups	60 s
Cooldown between scale-downs	120 s
Min replicas per stage n_{min}	1

D Action Validator and Constraints

Before executing any LLM-proposed action, SAIR applies the following validation rules to ensure safety and feasibility:

If the LLM proposes an action violating any constraint, the validator clamps the action to the nearest feasible value. For example, a proposed $\Delta n = +3$ is clamped to $+2$. Actions during cooldown periods are set to no-op for the affected stage.

E Reward Computation Pseudocode

Algorithm 2 Pareto Reward Computation

```

1: Input: context  $x$ , action  $a$ , Pareto frontier  $\mathcal{P}$ , SLA target  $T_{SLA}$ 
2: Weights:  $w_L = 0.7$ ,  $w_C = 0.3$ ,  $w_{proactive} = 0.3$ 
3: Measure  $L_{before}$ ,  $L_{after}$ ,  $C_{before}$ ,  $C_{after}$  after settling window
4:  $R_{lat} \leftarrow w_L \cdot (L_{before} - L_{after})/L_{baseline}$ 
5:  $R_{cost} \leftarrow -w_C \cdot (C_{after} - C_{before})/C_{budget}$ 
6: if  $L_{after} > T_{SLA}$  then
7:    $R_{SLA} \leftarrow -(L_{after}/T_{SLA})^2 + 1$  {Quadratic penalty}
8: else
9:    $R_{SLA} \leftarrow 0$ 
10: end if
11:  $\sigma \leftarrow \max(0, L_{p99}/T_{SLA} - 1)$  {Violation severity}
12:  $\mu \leftarrow \sum_i |\Delta n_i| + 0.5 \sum_i (|\Delta c_i|/\gamma_c$ 
13:    $+ |\Delta m_i|/\gamma_m + |\Delta \rho_i|) + 0.5|\text{scaled}|$ 
14:  $R_{proactive} \leftarrow \sigma \cdot \mu \cdot w_{proactive}$ 
15: Normalize:  $\tilde{L} \leftarrow L_{after}/L_{max}$ ,  $\tilde{C} \leftarrow C_{after}/C_{max}$ 
16: if  $(\tilde{L}, \tilde{C})$  is non-dominated in  $\mathcal{P}$  then
17:    $H \leftarrow$  hypervolume contribution w.r.t. ref. point  $(1, 1)$ 
18:    $R_{pareto} \leftarrow 1 + H$ 
19: else
20:    $d \leftarrow$  Euclidean distance to  $\mathcal{P}$  in  $(\tilde{L}, \tilde{C})$  space
21:    $R_{pareto} \leftarrow 0.8/(1 + d)$ 
22: end if
23:  $R \leftarrow R_{lat} + R_{cost} + R_{SLA} + R_{proactive} + R_{pareto}$ 
24:  $R \leftarrow \text{clip}(R, -R_{max}, R_{max})$  {Ensures Assumption 3.1}
25: Return  $R$ 

```

F Hyperparameters

Table 3: Hyperparameter settings for all experiments.

Parameter	Value
Context window size M	15 episodes
Reward threshold r_{min}	0
Pareto weight (latency) α	0.7
Pareto weight (cost) β	0.3
Diversity regularization λ_{div}	0.1
Initial exploration rate ϵ_0	0.15
Exploration decay λ	0.95
Minimum exploration ϵ_{min}	0.05
Decision interval	30 seconds

G Raw Cost Data

Table 4 presents the raw cost per 1000 requests for all experiments.

Table 4: Raw cost per 1K requests (\$, AWS on-demand: p3.2xlarge GPU, m5.xlarge CPU).

App	Pattern	Static	HPA	VPA	Thresh.	SAIR
ImgCls	Poisson	.058	.065	.070	.034	.024
	Ramp	.168	.185	.202	.081	.072
	Burst	.195	.267	.223	.127	.076
NLP	Poisson	.011	.008	.028	.014	.007
	Ramp	.038	.034	.047	.010	.009
	Burst	.028	.026	.012	.009	.009
TextGen	Poisson	.018	.017	.014	.014	.006
	Ramp	.012	.047	.188	.263	.007
	Burst	.012	.053	.013	.020	.007
Video	Poisson	.928	1.764	.704	.916	.530
	Ramp	1.764	2.520	.657	.691	.490
	Burst	1.411	1.411	1.642	1.010	.557

H Bottleneck Detection Metrics

Table 5 presents the per-class precision, recall, and F1-score for bottleneck detection.

Table 5: Per-class precision and recall for bottleneck detection.

Class	Precision	Recall	F1-Score
Preprocessing	87.0%	88.7%	87.8%
Inference	83.9%	89.7%	86.7%
Postprocessing	89.8%	91.7%	90.7%
Multiple	82.9%	70.7%	76.3%
Overall Accuracy	86.0%		

I Prompt Template

The SAIR agent uses a structured prompt with three components, implemented via DSPy [Khattab et al. \[2023\]](#) signatures. We reproduce the complete template below for reproducibility.

Input Fields.

- `sampled_episodes`: Past episodes formatted as learning history with reward labels. Each episode shows: context → action → reward.
- `current_input`: Current pipeline metrics formatted as stage-level statistics (replicas, queue depth, CPU/GPU utilization, allocated resources, end-to-end latency).
- `constraints`: Physical infrastructure limits and scaling guidelines (see below).

Output Schema. The LLM returns a structured JSON action:

```
{"preprocessing": {  
    "action": "scale_replicas"  
    | "scale_resources" | "scale_both"  
    | "none",  
    "replicas": <int>,  
    "cpu_millicores": <int>,  
    "memory_mb": <int>},  
    "inference": {  
        "action": "adjust_rate" | "none",  
        "rate_ratio": <float in [0,1]>},  
    "postprocessing": {  
        // same as preprocessing}}
```

Absolute-to-Delta Mapping. The LLM outputs *absolute* target values (e.g., `replicas: 3, cpu_millicores: 1000`). The executor converts these to deltas relative to the current state, then the action validator (Table 2) clamps each delta to the per-step discretization grid \mathcal{A}_i before execution. This ensures Assumption 3.4 holds: regardless of the LLM’s raw output, the executed action is always in \mathcal{A} .

Constraints Prompt (excerpt).

Physical Constraints: Max GPUs: 2, Max CPU cores: 64, Max cost budget: \$100/hour.

Scaling Guidelines: Current resource allocations are shown in state. Aggressive reduction (>50%) is dangerous. If $p99 > SLA$ and utilization is low, a burst already passed but the system failed to handle it; needs more capacity. Trust the latency: $p99 > SLA$ means the system failed.

Goals: Primary: Keep $p99$ latency below SLA target. Secondary: Minimize cost. Learn from outcomes: if scaling a stage didn’t improve latency, avoid scaling it next time.

Episode Format. Each in-context episode is formatted as:

Episode (Reward: +0.85 GOOD):

Input:

```
  preprocessing: replicas=2, queue=15  
    CPU_usage=78.3%, ...  
  inference: replicas=1, queue=3  
    GPU_usage=45.2%, rate_ratio=0.80  
  E2E Latency: p99=342ms
```

Prediction:

```
  {"preprocessing": {"action":  
    "scale_replicas", "replicas": 3},  
    "inference": {"action": "none"}}
```

Reward: +0.85

Episodes are ordered by reward (curriculum ordering) so the LLM observes a learning progression from lower to higher rewards.